IOSR Journal of Mechanical and Civil Engineering (IOSR-JMCE)
e-ISSN: 2278-1684,p-ISSN: 2320-334X, Volume 16, Issue 1 Ser. III (Jan. - Feb. 2019), PP 12-27
www.iosrjournals.org

Finite Element Modeling of Lateral Loads Resisting R.C. Cores of Irregular Shapes

Hisham A. El-Arabaty[1], Mohamed N. Fayed[2], Gamal H. Mahmoud[3], Akram M. Abdelmaksod[4]

[1] *(Structural Engineering Department, Faculty of Engineering/ Ain-Shams University, Cairo, Egypt)*
[2] *(Structural Engineering Department, Faculty of Engineering/ Ain-Shams University, Cairo, Egypt)*
[3] *(Structural Engineering Department, Faculty of Engineering/ Ain-Shams University, Cairo, Egypt)*
[4] *(Structural Engineering Department, Faculty of Engineering/ Ain-Shams University, Cairo, Egypt)*
Corresponding Author: Hisham A. El-Arabaty

Abstract: *Analysis of tall building under the effect of lateral loads is commonly performed using highly sophisticated commercial software finite element analysis packages. Reinforced concrete cores are among the structural elements used extensively to resist lateral loads. In order to account for concrete cracking, the design of these cores is performed using interaction diagrams, based on the relevant code idealization of the strain diagram throughout the section height. This idealization does not differentiate between cores of regular and irregular shapes. In addition, the torsional movements of these cores are not considered in computation of their ultimate capacity.In this research, an extensive study is conducted to investigate the actual structural behavior of cores of different section shapes, through the development of more accurate nonlinear finite element analysis models, taking into account steel yield, and concrete cracking. The parametric study includes analysis of symmetric and unsymmetric core shapes, and various degrees of torsional movements on the overall section capacity. The analysis results are compared to those obtained for the same sections using commonly used commercial software packages, and the differences are highlighted.The overall conclusions reached are used to make important recommendations regarding the "reduction factors" which need to be applied to the common interaction diagram design procedure, in case of cores of irregular sections in order to give designers a more realistic and accurate estimate of the core's ultimate carrying capacity.*

Keywords: *Finite Element Modeling, Reinforced Concrete cores, Nonlinear analysis, Cracked section analysis*

Date of Submission: 16-01-2019 Date of acceptance:02-02-2019

I. Introduction

Reinforced concrete structures are usualy designed to resist vertical loads with a system of slabs, beams, and columns. Also they are designed to resist lateral loads either through framing action between columns and beams or through reinforced concrete walls called shear walls and cores. Most of the time, framing action, shear walls, and cores are all used together as lateral loads resisting elements in a building. As architectrual considerations usually dictate the uses of different spaces in the building, structural engineers need to select lateral loads resisting elements which serve the architectural purposes. The selection of reinforced concrete core shapes is affected by the architectural plan, locations of stairs, elevators, and personal and material circulation. This could result in RC cores of regular or irregular shapes.

A review of the most commonly used software packages in the commercial market reveals that the analysis and design of these cores is performed similarly for all core shapes, without any differentiation between regular and irregular shapes. The objective of this paper is to study the actual behavior of RC cores of irregular shape under the effect of lateral loads and investigate whether they can be treated in design similar to cores of regular or whether they require a special treatment in design.

II. Problem Description

As most commercial software packages assume linear elastic behavior of structures in the analysis stage. However, when designing a core section, these programs apply the resulting straining actions to the section based on "Cracked Section" idealization. If the core section is modeled using a number of shell elements, the straining actions on these elements are combined together to produce a final bending moment, axial force, etc. on the whole section which is used for design.

The "Cracked Section" idealization adopted by design codes in general is based on applying a linear strain variation along the whole section height, with maximum compressive stresses at one end, and maximum tensile stresses at the other, regardless of its shape. For cores of regular shapes, this assumption is quite close to the actual section behavior. However, this is not the case for cores of irregular shapes.

(Figure 01) illustrates this concept clearly, as the stress distribution for the regular shape shown in (Figure 01-a) matches the traditional assumption of a full section uniform variation of strains, while a completely different behavior can be seen in (Figure 01-b), where the 2 vertical webs exhibit separate compression and tension zones, and the structural behavior diverges significantly from the traditional assumption.

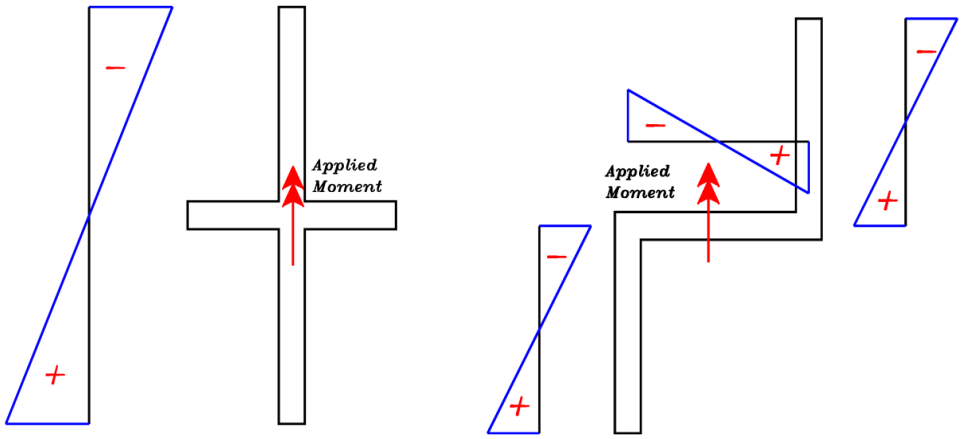

a) Regular core shape Irregular core shape

Figure1. Example of strain distribution through cores cross sections

The objective of this research is to utilize a more sophisticated non-linear analysis for a group of seleted section shapes for RC cores, to make an accurate assessment of the effect of this irregularity on the actual structural behavior of these cores, and to examine carefully the deviation observed in their actual behavior and ultimate carrying capacity as compared to results expected to be obtained for these sections using traditional commercial software packages.

III. Development of the Nonlinear Finite Element Model

3.1. ABAQUS Damaged Plasticity Model

ABAQUS software provides the capability of simulating the damage using either of the three crack models for reinforced concrete elements: (1) Smeared crack concrete model, (2) Brittle crack concrete model, and (3) Concrete damaged plasticity model. Out of the three concrete crack models, the concrete damaged plasticity model is selected in the present study as this technique has the potential to represent complete inelastic behavior of concrete both in tension and compression including damage characteristics.

The concrete damaged plasticity model assumes that the two main failure mechanisms in concrete are the tensile cracking and the compressive crushing (as explained at "ABAQUS Analysis User Manual – ABAQUS Version 6.11"). In this model, the uniaxial tensile and compressive behavior is characterized by damaged plasticity.

3.2. Numerical Model for Tensile Behavior of Concrete

In order to simulate the complete tensile behavior of reinforced concrete in ABAQUS, a post failure stress-strain relationship for concrete subjected to tension similar to (Figure 02) is used which accounts for tension stiffening, strain-softening, and reinforcement (RF) interaction with concrete.

To develop this model, the user inputs Young's modulus (E0), stress (σ_{to}), cracking strain (ε_t^{ck}) values and the damage parameter values (dt) for the relevant grade of concrete. The cracking strain (ε_t^{ck}) is calculated from the total strain using equation (1) below:

$$\varepsilon_t^{ck} = \varepsilon_t - \varepsilon_{0t}^{el} \qquad (1)$$

Where (ε_{0t}^{el})) is the elastic strain corresponding to the undamaged material, and (ε_t)) is the total tensile strain.

ABAQUS (SIMULIA) checks the accuracy of damage curve using the plastic strain values (ε_t^{pl}) calculated as in equation (2) below. Negative and/or decreasing tensile plastic strain values are indicative of incorrect damage curves which may lead to generate error massage before the analysis is performed (ABAQUS Manual, ABAQUS Version 6.11).

$$\varepsilon_t^{pl} = \varepsilon_t^{ck} \frac{d_t}{1-d_t} \frac{\sigma_t}{E_0} \qquad (2)$$

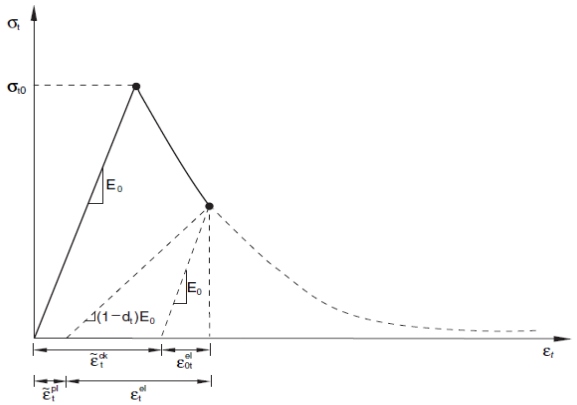

Figure2. Stress-Strain relation for concrete tension stiffening

There are different forms of tension stiffening models presented in the literature as reviewed. Concrete behavior in tension exhibits a linear rising branch up to the peak concrete tensile strength (σ_{to}). However, variation in the post-peak softening response significantly affects the efficiency of the numerical procedure (ease of convergence).

A schematic presentation for four tension softening idealizations considered in the literature is shown in (Figure 03): a bilinear softening response (Figure 03-a), a linear softening response (Figure 03-b), an exponential decay (Figure 03-c), and a constant softening response (Figure 03-d).

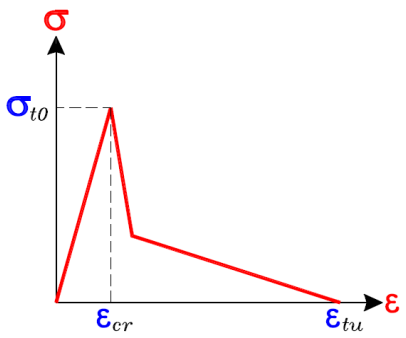

a) Bilinear Softening

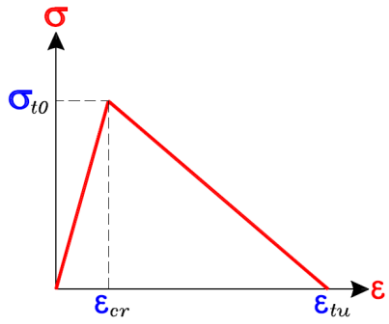

b) Linear Softening

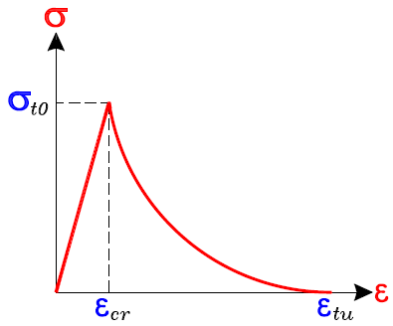

c) Exponential Softening

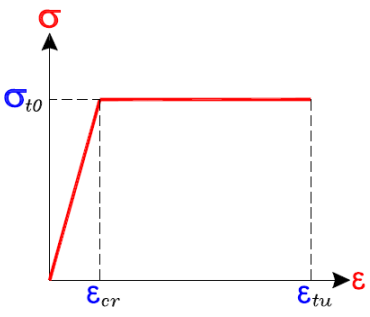

d) Constant Softening

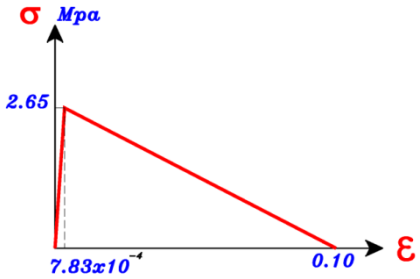

e) New idealization proposed for tension softening

Figure3. Idealizations for the concrete tensile behavior

The bilinear response was adopted by Genikomsou&Polak (2015) in their recent numerical application on punching shear in concrete slabs, using the concrete damaged plasticity in ABAQUS. Also the effect of a linear concrete tension softening behavior on the overall member response was previously adopted by Ellobody& Young (2011) in a numerical application to assess the nonlinear behavior of concrete-encased steel composite columns. The third representation considered is the exponential decay concrete softening response, proposed by Hordijk (1991). Similar to the above-described softening idealizations (linear and bilinear), the principle of the 'Fictitious Crack Model' suggested by Hillerborg et al. (1976) was also adopted in the Hordijk (1991) approximation, in which the crack-opening displacement is converted into a crack strain using the characteristic length (h). In addition, the constant softening behavior was discussed by Moharram (2018) in a study of the inelastic behavior of hybrid reinforced concrete beam and steel column systems.

A sensitivity analysis had been done by Moharram (2018) between the four tension softening idealizations considered to assess the balance between predictability and computational efficiency resulting from the three different responses. The study showed that the difference in load capacity and consequently the moment capacity of model is around 10 to 15% which is an acceptable deviation.

Several trials are performed for the selection of the appropriate idealization for this study. Trials showed that using linear, bi-linear, and exponential idealization resulted in convergence errors and lead to a stoppage of the model nonlinear analysis run, far before achieving the target compressive stress. Therefore, a new idealization for tension softening was proposed to be between constant and linear idealization as shown in (Figure 03-e). The new proposed idealisation is linear but with a relatively high value of (ε_{tu}), which means that in the relevant strain range, the tensile stresses are slightly reduced. In the current study, the concrete material had been selected with following values: (σto = 2.65 Mpa), and ($\varepsilon_{cr} = 0.0000783$))

3.3. Numerical Model for Compressive Behavior of Concrete

In order to define the stress-strain relation of concrete, user inputs the stresses (σ_c), inelastic strains (ε_c^{in}) corresponds to stress values, and damage properties (*dc*) with inelastic strains in tabular format. Therefore, total strain values are converted to the inelastic strains using equation (3) as shown:

$$\varepsilon_c^{in} = \varepsilon_c - \varepsilon_{0c}^{el} \qquad (3)$$

Where, $(\varepsilon_{0c}^{el}) = (\frac{\sigma_c}{E_0})$, (ε_{0c}^{el})= Elastic strain corresponding to theundamaged material and,

(ε_c) = Total tensile strain.

Furthermore,corrective measures are taken to ensure that the plastic strainvalues (ε_c^{pl}) calculated using equation (4) are neither negative nordecreasing with increased stresses. (ABAQUS Manual, ABAQUS Version 6.11)

$$\varepsilon_c^{pl} = \varepsilon_c^{in} \frac{d_c}{1-d_c} \frac{\sigma_c}{E_0} \qquad (4)$$

Typical compressive stress-strain relationship with damage properties and terms are illustrated in (Figure 04)

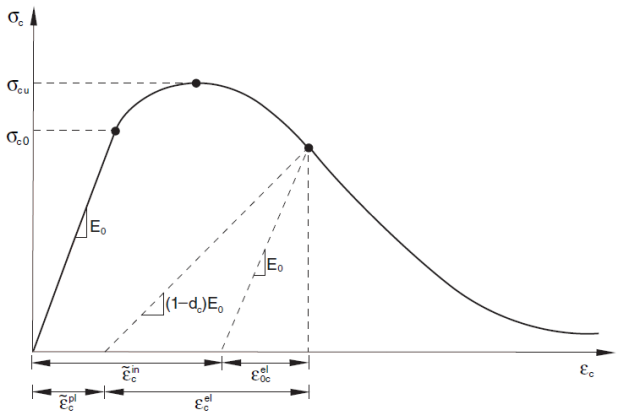

Figure4. Stress-Strain relation for concrete in compression from ABAQUS Manual

The complete stress-strain curve for concrete under compression used in this research study is derived using the experimentally verified numerical method by (CEN2004) which is summarized by the following equations:

$$\sigma_c = f'_c \frac{k\eta - \eta^2}{1+(k-2)\eta} \qquad (5)$$

$$k = \frac{1.05 E_{cm} |\varepsilon_{c1}|}{f'_c} \qquad (6)$$

$$\eta = \frac{\varepsilon_c}{\varepsilon_{c1}} \qquad (7)$$

Here (σ_c) and (ε_c) are the stress and strain of the compressive concrete, respectively; (f'_c) and (ε_{c1}) are the maximum compressive stress and the corresponding strain for standard cylinder test; (E_{cm})is the secant modulus of elasticity of concrete.

In flexural tests, values ranging from 0.0025 to 0.006 have been measured for (ε_u), it is usually assumed within the interval of 0.003 and 0.004. A value of ultimate strain (ε_u) is assumed at (ACI 318-14) and also at (ECP 203-2017) for flexural design of RC sections.

In this study, the concrete compressive material is selected with the following values: (f'_c = 39.2 Mpa), (ε_{c1}= 0.0018), (ε_u= 0.003), and (E_{cm}= 33840 Mpa). The stress-strain relationship used is shown in (Figure 05)

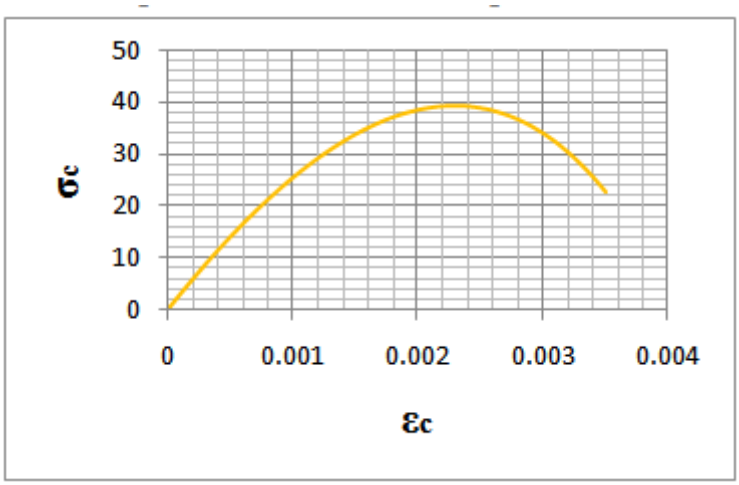

Figure5. Stress-Strain relation for concrete in compression used in this study

3.4. Other material properties

3.4.1. Damage parameters

The tensile damage parameter (d_t), and the compressive damage parameter (d_c) used in ABAQUS are defined as shownin equations (8) and (9), (Lubliner et al., 1989):

$$d_c = \begin{cases} Zero \rightarrow \varepsilon < \varepsilon_c \\ 1 - \frac{\sigma_\varepsilon}{f_c} \rightarrow \varepsilon \geq \varepsilon_c \end{cases} \quad (8)$$

$$d_t = \begin{cases} Zero \rightarrow \varepsilon < \varepsilon_{cr} \\ 1 - \frac{\sigma_\varepsilon}{\sigma_{to}} \rightarrow \varepsilon \geq \varepsilon_{cr} \end{cases} \quad (9)$$

Where (ε_c), (ε_{rc}) are the strains corresponding to the maximum uniaxial compressive and tensile stresses, respectively. (f_c) and (σ_{to}) denote the uniaxial concrete compressive and tensile strength, respectively. While (σ_ε) is the compressive or tensile stress corresponding to the calculated damage compressive or tension parameter.

3.4.2. Viscosity parameter

Effect of visco-plastic regularization is controlled using theviscosity parameter (v) which has an effect on the simulation results and convergence of the adopted models. Thisis a common technique used to overcome convergence difficulties by forcing the tangent stiffness matrix of the softening material to become positive for a very short time increment.

As a result, imposing minimum visco-plastic regularization helps improve the rate of convergence of the model. (Genikomsou&Polak, 2015) used values rangingfrom a minimum of $3x10^{-6}$ to a maximm of 0.0001 in situations where convergence becomes more demanding. A value of $3x10^{-6}$ has been selected for use in this research study. All other material properties are set to default values in ABAQUS

IV. Verifiction and Sensetivity Analysis

To investigate and verify the best technique to model the cores selected in this study using concrete damaged plasticity (CDP), one beam from a series of twelve conventional RC beam specimens tested by (Vecchio& Shim (2004)), and commonly referred to as the 'Toronto series', is used for calibration. Beam span length, cross-sectional dimensions, as well as the properties of concrete material used are presented in (Table 01).

Beam reference	Geometry				Concrete strength		
	b_w (mm)	h_c (mm)	L (mm)	l (mm)	f_c (MPa)	E_c (MPa)	f_{ct} (MPa)
B2	229	552	5,010	5,010	25.9	32,900	3.37

Table1. Geometrical details and concrete properties of the Toronto beam

The assessed beam had a rectangular cross-section, in which the overall concrete height (hc) and reinforcement depth (d) are hc=552mm and d=457mm, respectively. As indicated, metric-sized bars were adopted in this program for longitudinal and transverse reinforcement. M25 and M30 bars were used for the bottom longitudinal reinforcement. Three M10 bars were used for the compression reinforcement with transverse reinforcement; smaller rebars (D5) were used for the stirrups as shown in (Figure 06).

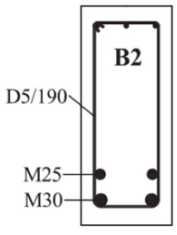

Figure6. Cross-sectional details of the Toronto RC test beam

Bar sizes in mm and their corresponding mechanical properties are provided in (Table 02). The specimen is centrally loaded in a three-point bending configuration. The load was applied vertically downwards in 40kN increments, followed by a displacement control close to ultimate. Details of the testing arrangement are given in (Figure 07).

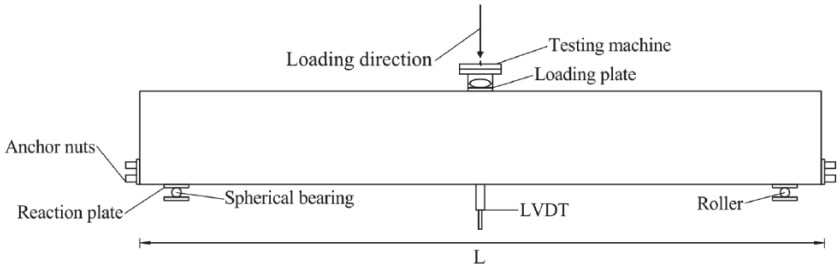

Figure7. Testing arrangement of the Toronto beam beam

Table 5.2 Steel properties of the Toronto series

Steel	Diameter (mm)	f_y (MPa)	f_u (MPa)	E_s(MPa)
M25[b]	25.2	445	680	220,000
D5	6.4	600	649	200,000

Table2. Steel properties for Toronto beam

The tested specimen is modeled using (CDP) in ABAQUS with two various techniques. In the first technique, concrete is modeled using four-noded shell element (S4R), whereas the longitudinal and transversal direction were modeled using rebar layers in shell elements. Spacing (S), and the area (A) which were used to determine the thickness of the equivalent rebar layer (t=A/S) as well as the angular orientation (α) of the rebar with respect to this local system.In addition, position of the rebars in the shell thickness direction measured from the mid-surface of the shell were specified (positive in the direction of the positive normal to the shell) Abaqus (2014).

The Beam was divided into three parts in elevation; first one was the lower part which extended from the center of bottom reinforcement to the end of concrete in tension side from one side and to a similar distance in the opposite direction. Second part was the upper part which extends from the center of top reinforcement to the end of concrete at compression from one side and to a similar distance at the other side. Third part was the middle one which is located between the upper and lower parts. The lower part simulates the longitudinal bottom reinforcement as well as the transversal shear reinforcement, while the upper one simulates the top reinforcement and also the shear reinforcement, and the middle part only simulates the shear reinforcement. Two supports had been carried out at the two ends of beam span; one of them is restraining the movement in X, Y, and Z directions while the other one is restraining the movement in Y, and Z directions only. Load had been applied at five points in Z direction which simulates the test plate length as shown in (Figure 08).

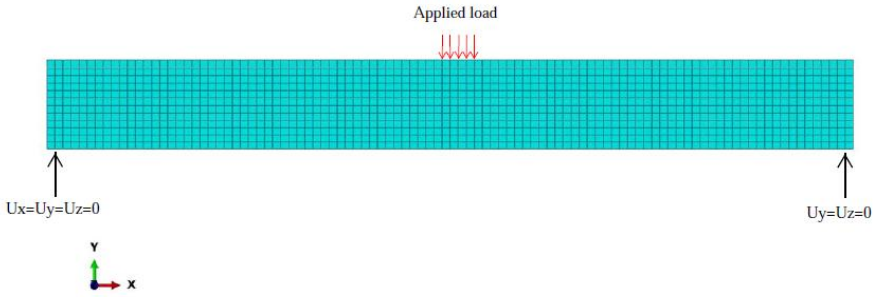

Figure8. Representation of the finite element model for the Toronto beam using shell elements

In the second technique, concrete was modeled using an eight-noded solid element (C3D8), whereas the reinforcement was modeled using the two-noded linear truss element (T3D2) in Abaqus (2014). Steel reinforcement and structural steel materials were modeled using a bilinear elasto-plastic model with strain hardening taken into account, for which the plastic modulus E_{sh} was approximately 1% of its initial elastic counterpart. A perfect bond condition between the reinforcement and concrete was considered using embedded

constraints. Load is applied at the nodes included within the area of the testing load plate. As technique one, two supports had been applied at the two ends. Representation of second technique model is shown in (Figure 09).

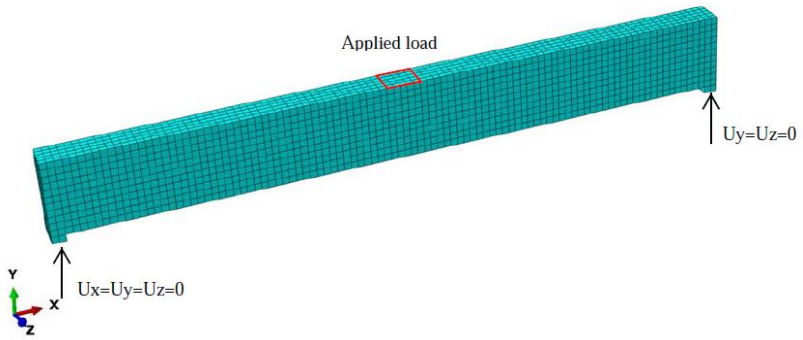

Figure9. Representation of the finite element model for the Toronto beam using solid elements

Failure load of the test specimen, as well as the failure loads obtained using the two modeling techniques (Shell and solid) is tabulated in (Table 03). The values verified the modeling technique of either shell or solid element to capture the failure load as the variation of results for the two techniques can be expected to be in an acceptable range. However, the failure load of the "SHELL ELEMENT" model is closer to the experimental test result (3% higher), while the failure load of the "SOLID ELEMENT" model is higher than the experimental test result by 10%. The first modeling technique ("SHELL ELEMENT" model) is selected for use in the current study.

	TEST	SHELL ELEMENT	SOLID ELEMENT
FAILURE LOAD (kN)	365	375	400

Table 03 . Failure load of Toronto test beam versus finite element models

V. Structural Behavior of Regular and Irregular Cores

The study plan for this research involves the simulation of RC cores of regular and irregular shapes under the effect of lateral loads, the main target being the accurate assessment of the ultimate moment capacity for cross sections of these cores, as compared to that obtained by the traditional interaction diagram assumptions utilized by commercial software packages.

Models of cantilever cores fixed at the base were developed and subjected to lateral forces at the free end of the cantilever. Simulationof the base fixation by preventing all deformaion at the points of fixation was found to result in local stress concentraions at points around the fixation, thus stopping the nonlinear analysis runs prematurely, and affecting the overall estimated lateral force, and thus the estimated section moment capacity.

A different simulation for the ground fixation is performed by adding a segment of the same core section but with higher wall thicknesses to provide a relatively rigid segment at below the base level. At the bottom of this rigid segment, fixation is achieved through Zero deformation restraints. This modification in the original model worked out as the failure at ultimate load occurred in the original segment, right at the top of the rigid segment, thus eliminating the effect of possible local stress concentrations. Several models were developed for the proposed study. All models are cantilevers with a height of 15 meters as shown in (Figure 10).

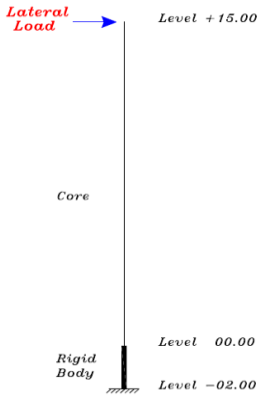

Figure10. Sketch for the core model simulation as cantilever

Two groups of models are proposed. Group (1) includes two models (1 and 2) as shown in (Figure 11). It is to be noted that both sections are identical in concrete dimensions and steel reinforcement. However Model (1) has a continuous web and Model (2) has a discontinuous web.

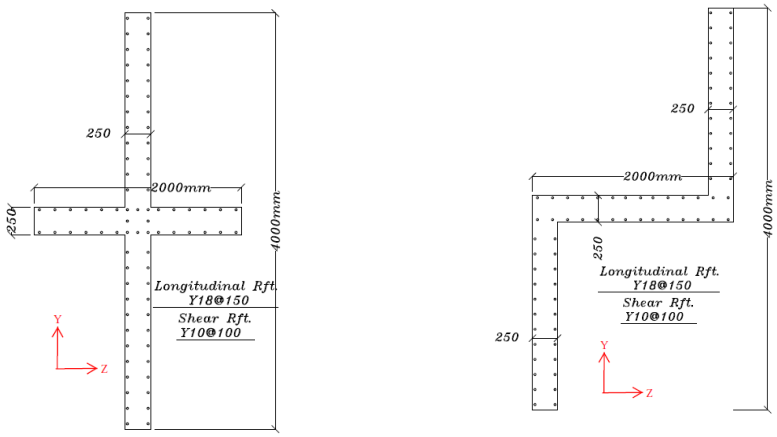

Model (1) Model (2)

Figure11. Cross sections of models (1) and (2) in Group (1)

Similarly, Group (2) includes two models (3 and 4) as shown in (Figure 12). In the same manner, both sections are identical in concrete dimensions and steel reinforcement, while the only difference is that Model (3) has a continuous web and Model (4) has a discontinuous web. This produces the I and Z shapes shown in (Figure 12) respectively. All Models 1 to 4 are free to rotate at their top without any restraint.

This selection was made so that Models 1 & 2 when analyzed using the traditional interaction diagram approach on any commercial software package would produce the same ultimate moment capacity. The same applies for Models 3 & 4.

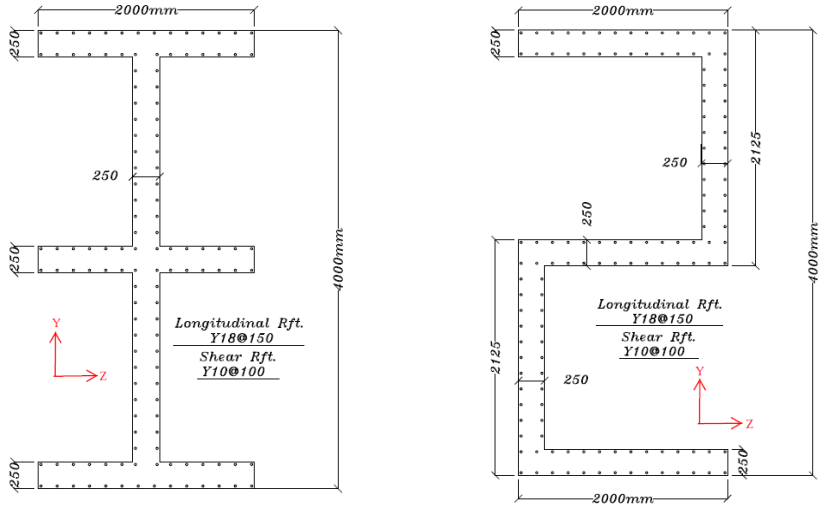

Model (3) Model (4)

Figure12. Cross sections of models (3) and (4) in Group (2)

Concrete for the whole core was modeled using a four-noded doubly curved shell element (S4R) with five integration points through the shell thickness, whereas steel reinforcement at the longitudinal and transversal directions were modeled using rebar layers in shell elements. Concentrated point load is acting at the center of gravity of core cross section at level +15.00 at Y direction. Fixation support is applied at level -2.00 which is the end of rigid body by restraining the three transitional degree of freedoms (Ux, Uy, and Uz) for all nodes. Tie constraint is used to contact the core with the rigid body using full contact at all nodes. In addition, coupling constraint is used to connect the point at which lateral load is acting to all points in its ZY plane with constraint degree of freedoms (Uy, Uz, and Rx). Static, Riks analysis had been performed to get the failure load

for the model and consequently, the moment capacity which is the target of this study. Representation for model (1) in group (2) is shown in (Figure 13) as an example.

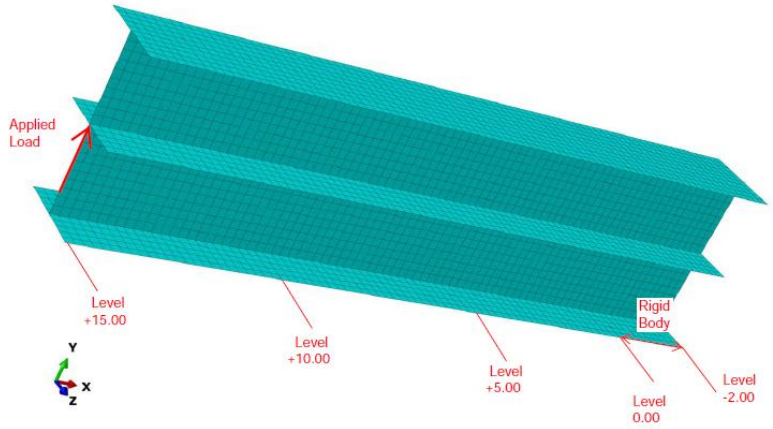

Figure13. Representation of finite element model for model (1) in group (2)

The structural behavior described by the previous models applies to reinforced concrete cores which are totally free to rotate at the top, while fixed at their bases. However, cores usually exist in buildings which include other structural elements. These elements serve to provide some degree of rotational restraint to the concrete floors, which in turn reduce the torsional rotation of the core sections. The degree of restraint depends on the stiffness and locations of these elements. Models 5 to 7 are developed with the purpose of studying the effect of this torsional restraint in detail.

(Figure 14) illustrates the selected section shapes, where a symmetrical section resembling an I-shape is used for Model 5. This section is totally symmetrical, and has a continuous web. For Model 6, an E-shaped section is selected. It has a continuous web, but is not symmetrical. Model 7 was selected as a Z-shape as shown. This model has a discontinuous web, and is not symmetrical.

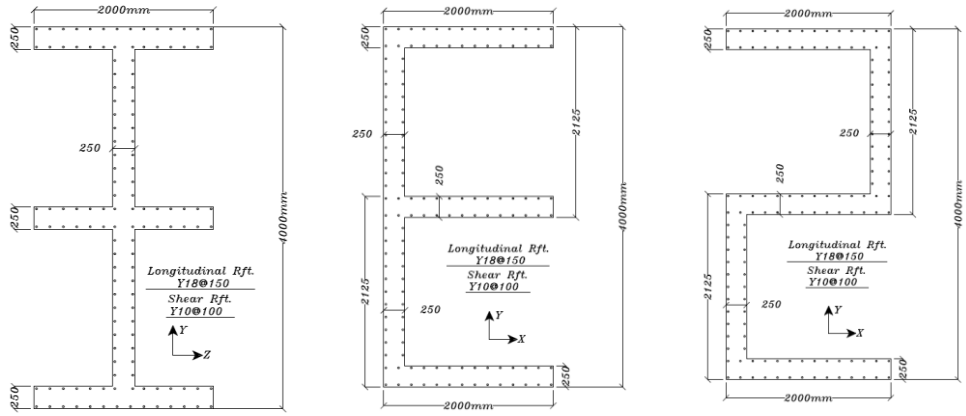

Model 5 (I-Shape) Model 6 (E-Shape) Model 7 (Z-Shape)

Figure14. Concrete dimensions and steel reinforcement of cores cross section for (I, Z, and E) models

VI. Results and Discussion

6.1 Stress and strain variation with load incrementation

(Figures 15 & 16)illustrate the stresses and strains obtained for a sample analysis run (Model 1). As shown in (Figures 15a & 15b), the variation of stresses and strains before cracking is uniform, with equal maximum strain values occurring at the top and bottom points of the section. The same applies to the stress variation.

When cracking starts to occur, the behavior starts changing and the strain variation shows a maximum tensile value at the section bottom higher than the maximum compressive value at the section top point, which means that the Neutral axis has started to move upward as shown in (Figure 16-a). Accompanying this change, a similar change in the stress diagram occurs, where yield stress starts to dominate the tensile zone (Figure 16-b), and extend upward more and more as the load increases and the section approaches failure. The results show that the model is simulating the actual concrete/steel section behavior accurately.

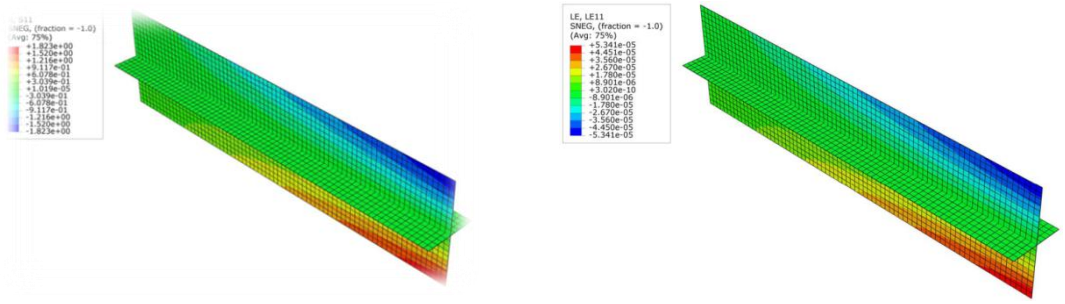

a) Stress contours b) Strain contours

Figure15. Stress and strain contours at longitudinal direction(before cracking) for model (1)

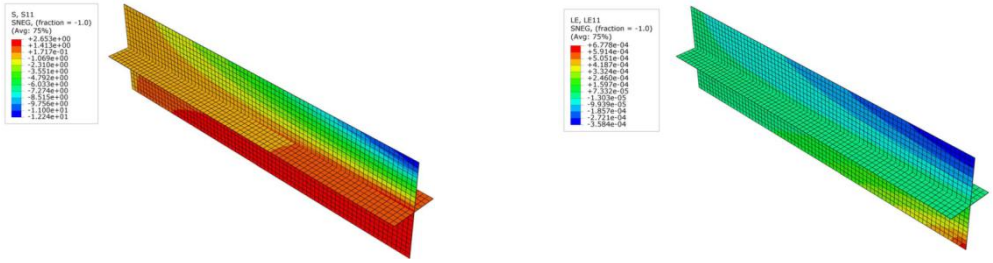

a) Stress contours b) Strain contours

Figure16. Stress and strain contours at longitudinal direction(after cracking)for model (1)

6.2 Effect of web discontinuity

Comparison of results obtained for Models 1 & 2 shows a very interesting phenomenon. For Model 1, (Figure 17) shows the stresses and strains at the failure stage. The continuous web produces a clear compression zone at the section top, where concrete reached crushing limit, while yield strains cover the bottom zone of the section. The maximum failure moment reached 19.2 MN.m.

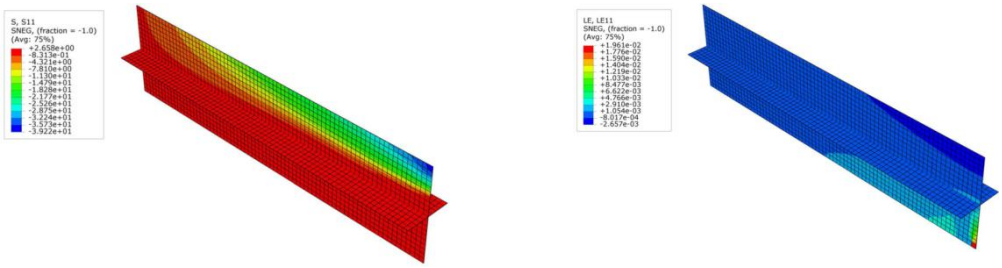

a) Stress contours b) Strain contours

Figure17. Stress and strain contours at longitudinal direction(at failure stage)for model (1)

The progress of Model 2 through the uncracked and cracked stages is illustrated in (Figures 18 to 20). The stress contours before cracking are shown in (Figure 18-a) which indicates that each web of the two webs connected by the flange has compressive stress at its top point and tensile stress at its bottom point which means that each web behaves in a similar manner to a single wall. However, there is a difference in stress distribution and stress values through the two webs as the upper web has a higher compressive stress at its top point compared to the lower web. On the contrary, the lower web has a higher tensile stress at its bottom point compared to the higher web. Moreover, the mid-height flange has compressive and tensile stresses at its right and left side respectively. The stresses through the section reach zero at three positions where they turned from compressive to tensile stresses, two of them at the webs while the third one is formed at the flange. Strain contours are also plotted in (Figure 18-b) with a similar distribution to stress.

By increasing the lateral load, concrete material starts to crack at the two tension sides which are the lower part of the higher web accompanied with a part of flange and the lower part of lower web. After cracking, it is noted that the maximum compressive stress through the section has started to form at the top point of the lower web instead of the top point of the higher web. The Neutral axis for each web has started to move upward, as shown in the strain variation (Figure 19-b). At the failure stage, the compressive stress at the top point of the lower web has reached the maximum value as shown in (Figure 20-a). The maximum failure moment reached 10.3 MN.m.

The results obtained for Models 1 & 2 resemble very closely the strain variation outlined in figure 01, which illustrates clearly the difference in section behavior. From the above results, it can be seen that the irregularity of the core shape in Model 2, produced by the discontinuous web, has produced a significant reduction in the ultimate moment capacity of the section. (46% decrease). Analysis of the same 2 shapes using a commercial software package was found to produce the same exact ultimate moment capacity for both shapes. This clearly shows that the code assumptions upon which commercial packages are based do not capture the actual structural behavior of such irregular shaped reinforced concrete cores.

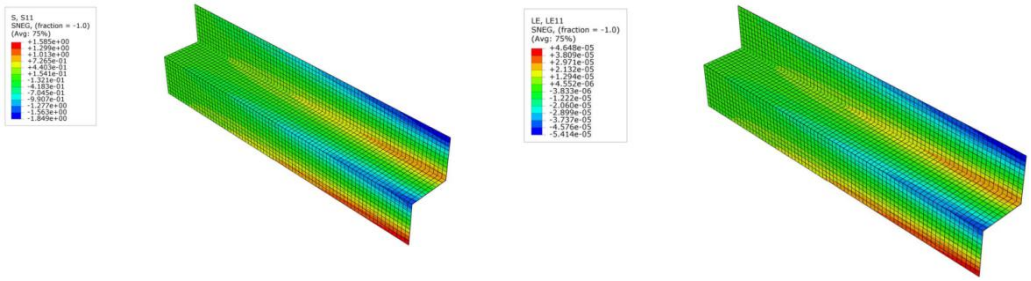

a) Stress contours b) Strain contours

Figure18. Stress and strain contours at longitudinal direction(before cracking) for model (2)

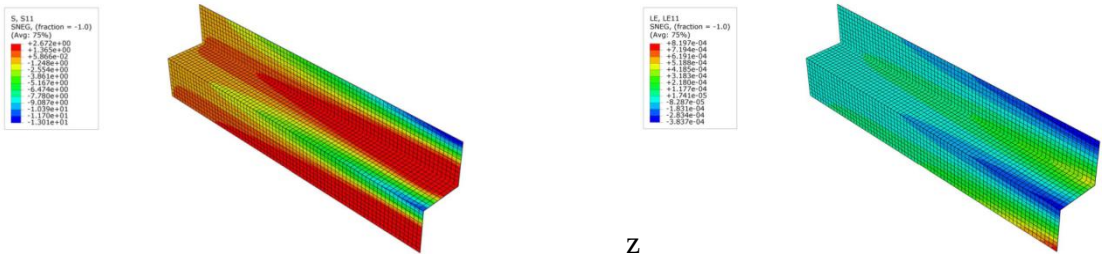

a) Stress contours b) Strain contours

Figure19. Stress and strain contours at longitudinal direction(after cracking) for model (2)

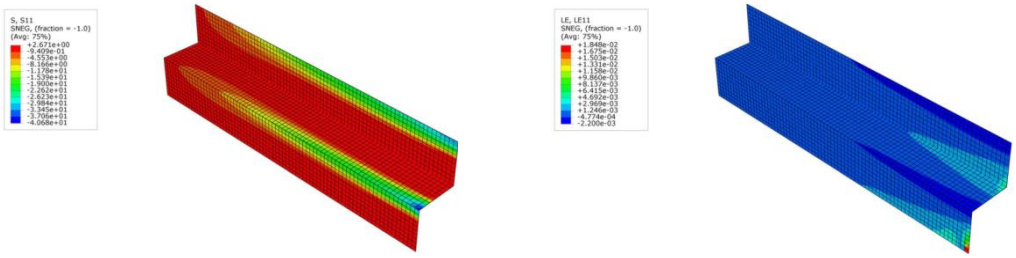

a) Stress contours b) Strain contours

Figure20. Stress and strain contours at longitudinal direction(at failure stage) for model (2)

Models 3 & 4 results show a similar pattern of behavior to that seen for Models 1 &2. The 2 models (3&4) have the same properties, except for the web which is continuous for Model 3, and discontinuous for Model 4. (Figure 21) shows the stress variation in Model 3 section after cracking. The analysis results are shown in (Figure 21-a), while a schematic diagram gives a clear illustration of the stress (and strain) variation in the section (Figure 21-b).

Similarly, for Model 4, (Figure 22) illustrates the stress variation. It can be seen that the stress pattern does not conform to the traditional assumption of full section linear variation, as the 2 webs show separate behavior, and 2 compression and tension zones can be clearly seen in the section. This reflects on the overall bending moment capacity of the section, as the ultimate moment capacity is 33.8 MN.m for Model 3, and 23.9 MN.m for Model 4. The difference caused by the section irregularity is around 30%. Analysis of the same models using software packages "SP COLUMN", and "ETABS" produces exactly the same ultimate moment capacity for both models, which highlights the fact that the code assumptions applied in these programs do not capture the actual structural behavior of the section in case of this irregular shape.

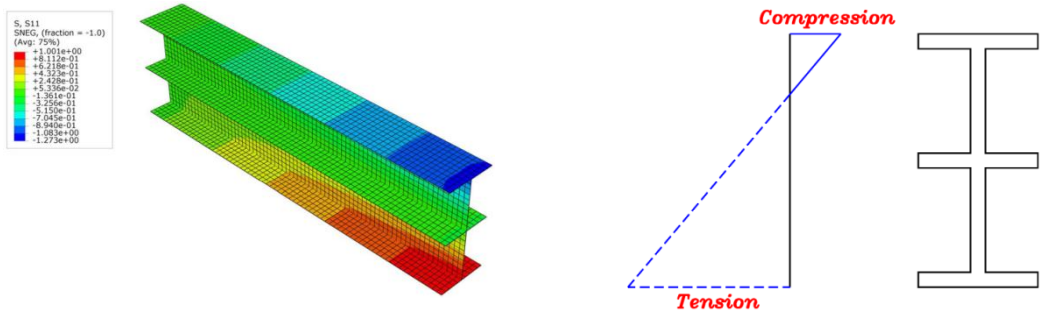

a) ABAQUS Results b) Schematic diagram

Figure21. Stress contours (after cracking) for model (3)

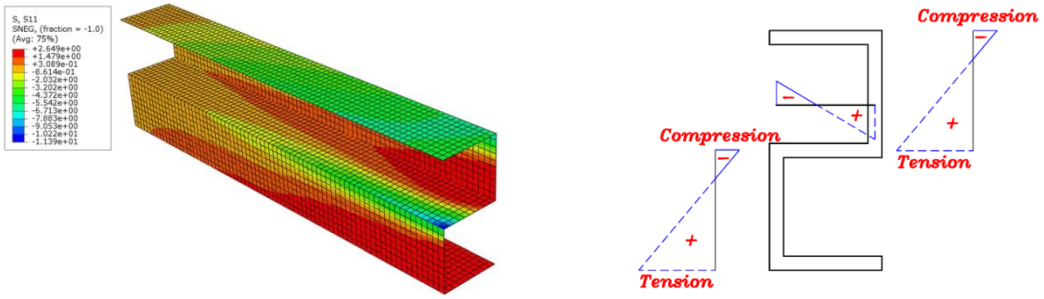

a)ABAQUS Results b)Schematic diagram

Figure22. Stress contours (after cracking) for model (4)

6.3 Effect of torsional restraint

As explained in section 5, 3 different sections of (I, Z, and E) shapes were selected for models 5, 6 & 7 respectively. Two cases were applied to each section, as shown in (Table 04). As shown, in cases 5A, 6A & 7A , the core is allowed to rotate freely, without any restraint, while in cases 5B, 6B & 7B, the core is restrained at several heights to prevent its rotational movement (thus simulating the effect of strong structural elements surrounding the core, and preventing its in-plane rotation by fixing the slab in place.

MODEL	**5**		**6**		**7**	
Type	A	B	A	B	A	B
Shape	I		E		Z	
In-plane rotation restraint	Fully restrained in-plane rotation	Free to rotate	Fully restrained in-plane rotation	Free to rotate	Fully restrained in-plane rotation	Free to rotate

Table4. Specifications of models used to study the effect of torsion

(Figures 23, 24 and 25) show the variation of stresses along the different sections (I, E & Z-shaped) obtained from the nonlinear analysis of Models 5, 6 & 7 respectively. (Table 05) summarizes the results of the nonlinear analysis of the 6 Models described above. As shown in the table, the I-section results are not affected by the rotational restraint. This is obviously due to the symmetrical shape of the section. In addition, its continuous web causes the section to develop the highest ultimate moment capacity within all selected sections. This moment capacity of the I-section (33.8 MN.m) will be considered a reference for comparison to other sections capacity.

The E-section behavior is different from the I-section. While the restrained case ultimate capacity is very close to that of the I-section, the unrestrained case shows a significantly reduced ultimate capacity (22.2 MN.m), which is 34% less than the I-section capacity. This can be explained by the fact that the shear center of the E-section does not coincide with its CG, thus the section rotates significantly, producing additional stresses in the flanges of the section, which cause failure at a reduced moment value.

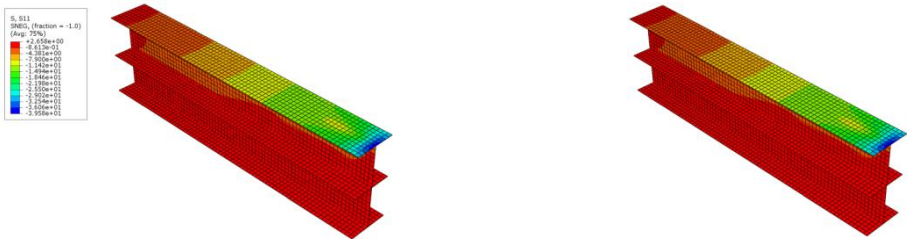

(a) In-plane rotation restrained (b) Free to rotate in-plane

Figure23. Stress contoursat failure stage for model 5 (I-Shape)

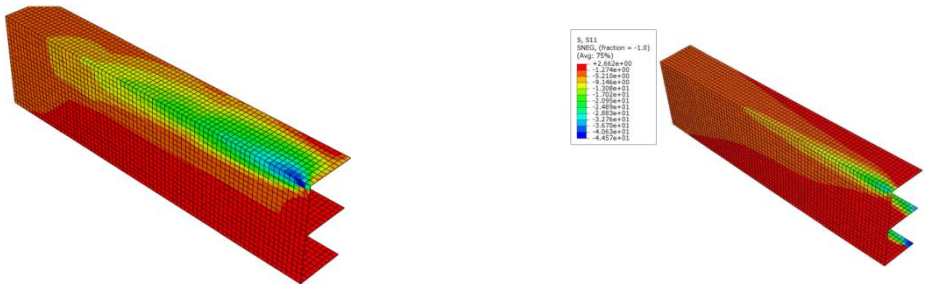

(a) In-plane rotation restrained (b) Free to rotate in-plane

Figure24. Stress contoursat failure stage for model 6 (E-Shape)

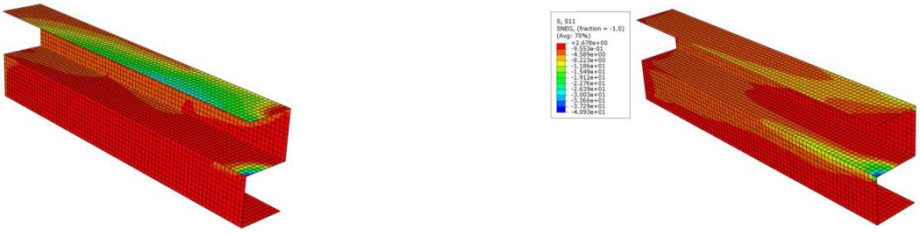

(a) In-plane rotation restrained (b) Free to rotate in-plane

Figure25. Stress contours at failure stage for model 7 (Z-Shape)

MODEL	5		6		7	
Type	A	B	A	B	A	B
Shape	I		E		Z	
In-plane rotation restraint	Fully restrained in-plane rotation	Free to rotate	Fully restrained in-plane rotation	Free to rotate	Fully restrained in-plane rotation	Free to rotate
In-plane rotation at top level of core (radians)	0	0	0	0.026	0	0.07
Ultimate moment capacity (MN.m)	33.7	33.7	28.1	23.9	33.1	22.1
Ultimate moment capacity (MN.m)	0	0	16.6	29	1.8	33

Table5. Ultimate moment capacity and in-plane rotation for models 5, 6, and 7

The rotation magnitude and the resulting displacements obtained from analysis in the E-section for the unrestrained case are shown in (Figure 26). As seen in the figure, a rotation of 0.07 radians occurs, accompanied by large horizontal displacements in the flanges. The magnitudes of these displacements are comparable to the vertical displacement, and produce significant changes in the stress distribution in the section, thus causing failure to occur at a relatively low value of moment capacity.

As for the Z-section, it can be seen in (Table 05) that the ultimate capacity for the "torsionally restrained" case has been reduced relative to the reference capacity of the I-section. The ultimate moment capacity of 28.1 MN.m is 17% less than that of the I-section. This can be explained by the effect of the discontinuous web of the section, producing different compression and tension zones in both of the section webs.

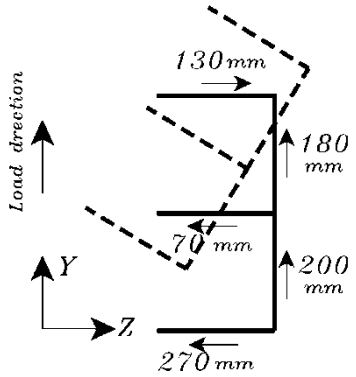

Figure26. Displacement of core walls at their long direction at failure stage for model 6-b (Free to rotate)

More reduction in ultimate moment capacity is observed for the case of the "torsionally unrestrained" case (Model 7B), reaching a value of 23.9 MN.m which is 29% less than the capacity of the reference I-section. This reduction is a result of 2 factors acting together, namely the discontinuity of the web, and the torsional movement of the section.

The torsional movement of the section is illustrated in (Figure 27), where the displacements resulting from the analysis of Model 7B are shown. The large lateral movements of the flanges (especially the bottom flange) can be seen, and have a significant effect on the section behavior and its ultimate moment capacity.

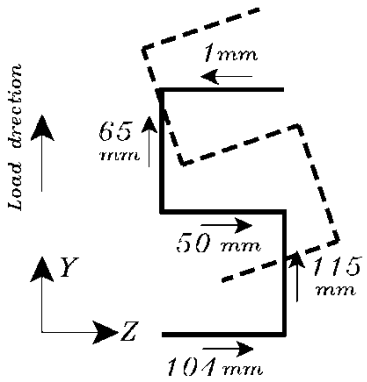

Figure27. Displacement of core walls at their long direction at failure stage for model 7-b (Free to rotate)

Analysis runs of all 6 models above using "SP COLUMN", and other programs yielded the same moment capacity for all 6 shapes. This is caused by the fact that the linear strain assumption throughout the whole section height prevents any assessment of the effect of web discontinuity, and any other irregularity in shape. Moreover, commercial software packages calculate the total straining actions on the core section by accumulating the individual forces acting on all elements at the section. This prevents any consideration of the effect of the torsional movement which affects the stresses in the different flanges of the section differently. These observations indicate a critical deficiency in the code assumptions on which commercial software packages base their design routines, and indicate a strong need for introducing capacity reduction factors to address these factors which are currently not accounted for.

VII. Summary and Conclusions

- In this study, the common assumptions related to design of cracked sections used by commercial software packages, are investigated in relation to their application in estimating the ultimate capacity of reinforced core sections, in tall buildings under the effect of lateral loads, with an emphasis on the modeling of cores of irregular shapes, and cores which undergo torsional movements.
- A sophisticated nonlinear finite element analysis models is developed for the analysis of reinforced concrete cores under the effect of lateral loads. Verification of the proposed model is performed using published experimental data, and the model results were found to be in very good agreement with experimental results.
- Analysis results obtained showed high agreement between the structural behavior of symmetric regular core sections (I-section, etc), and the full-height linear strain assumption specified by design codes, and applied in commercial software packages.

- In case of irregular core shapes, especially where the section web is discontinuous (Z section, etc), the structural behavior and the resulting stress and strain distribution are highly different from the common linear strain assumption. The effect on the ultimate moment capacity of the section is found to be significant, and reached up to 46% reduction in capacity for some sections. This reduction in capacity was found to be smaller when the core section is rotationally restrained, and was found to be largest for the case of rotationally unrestrained core sections.
- The analysis results showed that commercial packages design routines produced the same results for regular and irregular core shapes, and the results also did not reflect the effect of torsional movements. This is caused by the fact that the linear strain assumption throughout the whole section height prevents any assessment of the effect of web discontinuity, and any other irregularity in shape. Moreover, commercial software packages calculate the total straining actions on the core section by accumulating the individual forces acting on all elements at the section. This prevents any consideration of the effect of the torsional movement which affects the stresses in the different flanges of the section differently. These observations indicate a critical deficiency in the code assumptions on which commercial software packages base their design routines.
- A main recommendation is reached in this study regarding the necessity for introducing capacity reduction factors to the computed ultimate moment capacity of core sections. An extensive parametric study including various common core shapes, and different levels of rotational restraint is required to reach adequate reduction factors for the accurate assessment of the ultimate capacity of core sections in highrise buildings.

References

[1]. ABAQUS Manual, ABAQUS Version 6.11.

[2]. ACI Committee, American Concrete Institute and International Organization for Standardization, 2008. Building code requirements for structural concrete (ACI 318-08) and commentary. American Concrete Institute.

[3]. CEN (ComitéEuropéen de Normalisation). 2004. Eurocode 2: Design of Concrete Structures – Part 1: General Rules and Rules for Buildings, EN 1992-1-1:2004. Brussels:CEN. 230 p.

[4]. ECP 203 (2012), "Egyptian Code of Practice for Design and Construction of Reinforced Concrete Structures 2012.".

[5]. Ellobody, E. and Young, B., 2011. Numerical simulation of concrete encased steel composite columns. *Journal of Constructional Steel Research, 67(2), pp.211-222.*

[6]. Genikomsou, A.S. and Polak, M.A., 2015. Finite element analysis of punching shear ofconcrete slabs using damaged plasticity model in ABAQUS. Engineering Structures, 98, pp.38-48.

[7]. Hillerborg, A., Modéer, M. and Petersson, P.E., 1976. Analysis of crack formation and crack growth in concrete by means of fracture mechanics and finite elements. Cement and concrete research, 6(6), *pp.773-781*.

[8]. Hordijk, D.A., 1991. Local approach to fatigue of concrete (Doctoral Dissertation, Delft University of Technology)

[9]. Lubliner, J., Oliver, J., Oller, S. and Onate, E., 1989. A plastic-damage model for concrete. *International Journal of solids and structures, 25(3), pp.299-326.*

[10]. Moharram, M., 2018. Inelastic Behaviour of Hybrid Reinforced Concrete Beam and Steel Column Systems. (Doctoral Dissertation, Imperial College of Science, Technology and Medicine, London,)

[11]. Vecchio, F.J. and Shim, W., 2004. Experimental and analytical reexamination of classic concrete beam tests. *Journal of Structural Engineering, 130(3), pp.460-469.*

Hisham A. El-Arabaty "Finite Element Modeling of lateral loads resisting R.C. cores of Irregular shapes." IOSR Journal of Mechanical and Civil Engineering (IOSR-JMCE) , vol. 16, no. 1, 2019, pp. 12-27.